2016 IEEE International Conference on Robotics and Automation (ICRA)
Stockholm, Sweden, May 16-21, 2016

Narrow Passage Sampling in the Observation of Robotic Assembly Tasks

Korbinian Nottensteiner[1] , Mikel Sagardia[1], Andreas Stemmer[1], and Christoph Borst[2]

Abstract— **The observation of robotic assembly tasks is required as feedback for decisions and adaption of the task execution on the current situation. A sequential Monte Carlo observation algorithm is proposed, which uses a fast and accurate collision detection algorithm as a reference model for the contacts between complex shaped parts. The main contribution of the paper is the extension of the classic random motion model in the propagation step with sampling methods known from the domain of probabilistic roadmap planning in order to increase the sample density in narrow passages of the configuration space. As a result, the observation performance can be improved and a risk of sample impoverishment reduced. Experimental validation is provided for a peg-in-hole task executed by a lightweight-robot arm equipped with joint torque sensors.**

I. Introduction

Typical assembly processes consist of sequences of various contacts transferring parts from free configuration space to constrained goal configurations. In robotic assembly execution (Fig. 1), the observation of such processes is required to detect and handle errors, adapt action parameters and robot controllers, or even to learn strategies and perform high-level reasoning. A major goal of assembly observation is to provide information about partially hidden states, e.g. geometric uncertainties or contact states. In recent years, especially sequential Monte Carlo (SMC) approaches showed their advantages in the observation of robotic assembly processes. The SMC framework allows not only to deal with non-linear models, but also with non-Gaussian and multi-modal distributions, cf. [1] and [2], which are obviously present when multiple contact states are possible. Within this probabilistic framework, state estimates are obtained by the sequential propagation, weighting and selection of a set of samples according to their consistency with the sensory information and the assumed system and measurement models.

In particular, Chhatpar and Branicky [3] propose a probing based localization method and demonstrate it in a lock-key assembly. Hypotheses of relative poses are initially spread in a pre-generated map of the configuration space and further updated by subsequent probes until the samples converge, i.e. the lock is localized. Thomas et al. [4] also apply pre-generated maps to localize the parts in an assembly task. The so-called force-torque maps contain additional information about expected contact forces and torques, which is used as further input in the weighting of the samples. A drawback of the pre-generated maps is the high preparation effort needed to ensure completeness in a sufficient level of detail.

[1] Institute of Robotics and Mechatronics (RMC-RM), German Aerospace Center (DLR), 82234 Wessling, Germany
[2] KUKA Roboter GmbH, 86165 Augsburg, Germany
Contact: korbinian.nottensteiner@dlr.de

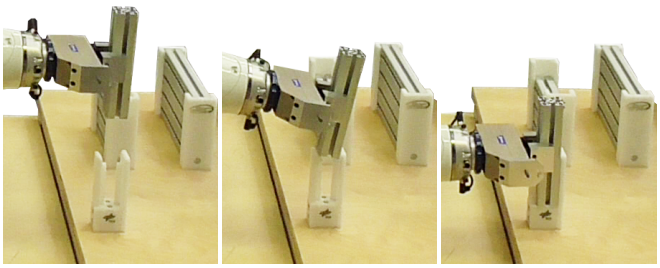

Fig. 1. Peg-in-hole insertion of an aluminum profile into an assembly fixture with a LWR robot arm. The peg is tilted, aligned in contact and inserted with impedance control.

Further SMC approaches use contact state graphs [5], which add a higher semantic layer to the observation by partitioning the configuration space into distinct regions, so-called contact formations. The knowledge of the properties and the transitions between certain contact formations can then be used to improve the performance of the observation algorithm [6] or resolve ambiguous force and torque measurements [7]. While these methods perform well, it is not clear how they scale to realistic examples, as they are only demonstrated for simple geometrical objects with a few possible contact states.

A general issue of the SMC methods is the number of samples required for reliable observation results, what consequently becomes a question of computational resources for high state dimensions and complex models. Taguchi et al. [8] reduce the number of samples significantly by the help of a Rao-Blackwellized particle filter (RBPF) that combines a sample based position estimation with a Kalman filter for orientation uncertainties. The additional usage of vision systems to initialize the sample distribution [9] or the fusion of tactile and vision measurements, [4] and [10], can also help to improve the observation performance. Although progress has been made, problems remain in cases with highly constrained configurations, as also concluded in [10]. Especially the transitions from free space into narrow passages in the configuration space, as in peg-in-hole assembly tasks, are still challenging with respect to sample impoverishment. This particular effect is characterized by the selection of only a few high-weighted samples in the resampling step. In the further observation, the samples might then not be sufficient to approximate the full posterior distribution and thus lead to strong biases in the estimates.

Avoiding the narrow passage during the localization, which is suggested by [3] and [8] by probing before the insertion, is not always feasible considering practical constraints

in real applications, and focuses not on the observation of the actual assembly process. Therefore, in the presented work, the particular cases of transitions into narrow passages before the final convergence of the sample set are considered, and two alternative sampling policies are compared with the commonly used random motion model. Both policies are rooted in probabilistic roadmap planning (PRM, [11]) and are used here for the first time in the context of sampling based observation of assembly processes. The Gaussian sampler [12] allows the generation of higher sample densities near the border of the configuration space. The random bridge builder (RBB), presented by [13], increases the sample density especially in narrow passages. By increasing the density in these critical regions a reduced risk of sample impoverishment and a higher performance is expected.

The sampling policies are adapted and integrated directly in the propagation model of the SMC algorithm. Here, the configuration space is sampled locally around each contact hypothesis and thus only the relevant space is considered and no pre-generated maps are required. As a contact model, the voxelmap-pointshell algorithm (VPS, [14]) is used, which is a penalty based collision algorithm, commonly used in haptic rendering for the computation of contact forces. Our fast and generic implementation [15] of the VPS is able to handle complex geometries given as CAD data. The developed observation framework is experimentally validated with sensory information of a lightweight-robot arm (LWR) executing a peg-in-hole task with complex shaped aluminum parts. The measurements include the current joint position and torques and therefore allow for the observation of contact states. The LWR is able to robustly execute such peg-in-hole tasks by the help of the impedance control mode [16]. But, on a higher abstraction level, these assembly strategies are feed-forward controllers, which do not directly incorporate the current state of the execution and thus are not capable of adapting the strategy to the current situation. This motivates the presented observer algorithm that monitors the assembly progress and provides state information for high level controllers and reasoning systems in future applications that increase the overall performance of the assembly system.

The work is presented as following, the applied robot and contact models are presented in Section II, together with the observation framework, and followed by the description of the sampling policies in the propagation step in Section III. Simulations and experimental results are provided for a peg-in-hole insertion in Section IV. Finally, the results are discussed in Section V and concluded in Section VI.

II. Models for Contact Observation

In contact tasks, the uncertainties from the robot arm combine with further uncertainties in the kinematic chain, which is closed in the contact between an environment object (EO) and a manipulated object (MO). In this section, the robot and uncertainty models are presented, as well as the contact models used for the observation of the assembly task. An overview of the observation framework is given, for which different sampling policies are investigated later.

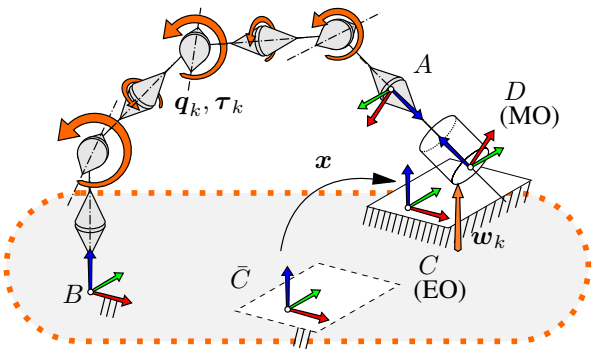

Fig. 2. Kinematic chain consisting of the robot flange A, the base B, the initial reference frame $\bar{C}$ and the frame C of the EO, and the frame D of the MO. The geometric uncertainties are summarized in the state $\boldsymbol{x}$ as parameter in the transformation $\boldsymbol{H}_{\bar{C}C}$. The contact wrench $\boldsymbol{w}_k$ induces a torque $\boldsymbol{\tau}_k$ in the robot joints; together with the current robot configuration $\boldsymbol{q}_k$ the state $\boldsymbol{x}$ is estimated.

A. Robot and Uncertainty Model

A general formalism on how to model the uncertainties in a kinematic chain can be found in [17]. As the observation of the assembly task is in focus of this work, not the identification of individual uncertainties is of interest, but rather the cumulative relative uncertainty between MO and EO, where the kinematic chain will be closed during the assembly. Exemplary in this work, the state $\boldsymbol{x} \in \mathbb{R}^m$ shall therefore be defined as geometric uncertainty in the transformation $\boldsymbol{H}_{\bar{C}C}(\boldsymbol{x}) \in SE(3)$ between an initial reference pose $\bar{C}$ and the actual pose C of the EO. It is assumed that the EO and MO are statically fixed to the environment and the robot, respectively. In the nominal case, $\boldsymbol{x}$ contains $m \leq 6$ constant, but unknown parameters affecting positions and orientations. In the real case, the specific source of uncertainty vanishes within the state $\boldsymbol{x}$, i.e. inaccurately known object poses or model errors are not separable without adding further error models in the relevant parts of the kinematic chain. The here chosen approach of a cumulative uncertainty is reasonable as long as unmodelled effects in the remaining kinematic chain are bound on a small scale. Note also that the presence of unmodelled effects, e.g. a not completely fixed EO, can produce a time varying state. Therefore, the state value at a specific instant of time k will be denoted as $\boldsymbol{x}_k$.

A rigid body model of the robot arm is assumed. The forward kinematics are then given by the transformation function $\boldsymbol{H}_{BA}(\boldsymbol{q}) \in SE(3)$ with the joint configuration $\boldsymbol{q} \in \mathbb{R}^n$, where B represents the base and A the flange of a robot arm with $n \geq 6$ degrees of freedom (Fig. 2). The MO is attached to the robot flange with a known and fixed transformation $\boldsymbol{H}_{AD} \in SE(3)$, where D is the coordinate system of the MO. At time k, the relative pose $\boldsymbol{H}_k := \boldsymbol{H}_{CD} \in SE(3)$ between MO and EO is obtained for a given state $\boldsymbol{x}_k$ and the current joint configuration $\boldsymbol{q}_k$ from the closed kinematic chain by

$$\boldsymbol{H}_k(\boldsymbol{q}_k, \boldsymbol{x}_k) = \boldsymbol{H}_{C\bar{C}}(\boldsymbol{x}_k)\boldsymbol{H}_{\bar{C}B}\boldsymbol{H}_{BA}(\boldsymbol{q}_k)\boldsymbol{H}_{AD}, \quad (1)$$

where $\boldsymbol{H}_{\bar{C}B}$ is given by the inverse of the initially assumed

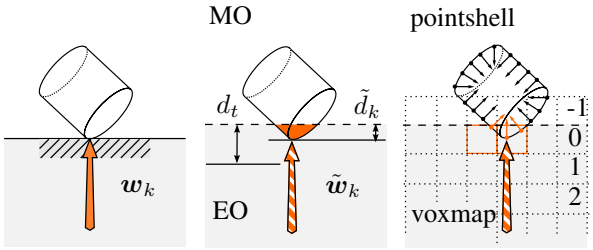

Fig. 3. (a) Real contact situation. (b) Contact model. (c) Implementation of contact model with VPS. $\tilde{d}_k$ denotes the contact distance and d_t a threshold on the maximal feasible virtual penetration, $\tilde{\boldsymbol{w}}_k$ the virtual contact wrench.

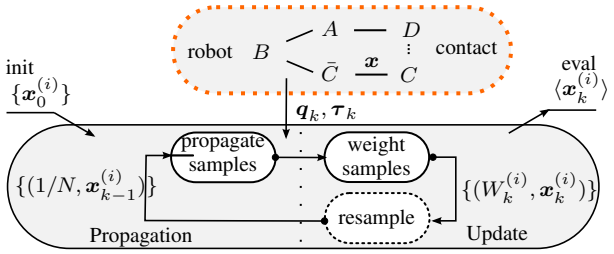

Fig. 4. The observation cycle of the basic SMC algorithm applied for assembly observation. Hypotheses $\{\boldsymbol{x}_k{}^{(i)}\}$ with $i = 1, ..., N$ of the state $\boldsymbol{x}$ in the kinematic chain of the robot, are propagated, then weighted according their consistency with the measurements and finally resampled.

pose $\boldsymbol{H}_{B\bar{C}} \in SE(3)$ of the EO relative to B, see Fig. 2.

The considered robot arms are equipped with torque sensors in their joints. When MO and EO are in contact, a torque $\boldsymbol{\tau}_k \in \mathbb{R}^n$ can be obtained from the intrinsic sensors, which is dependent on the robot configuration by the well known relation:

$$\boldsymbol{\tau}_k = \boldsymbol{J}_k^T \boldsymbol{w}_k, \tag{2}$$

where $\boldsymbol{J}_k := \boldsymbol{J}_{BD}^D(\boldsymbol{q}_k) \in \mathbb{R}^{6 \times n}$ is the Jacobian of the robot arm with respect to D and the external wrench $\boldsymbol{w}_k :=_D \boldsymbol{w}_k = (\boldsymbol{F}_k{}^T, \boldsymbol{M}_k)^T)^T \in \mathbb{R})^6$ acting on the MO at D.

B. Virtual Contact Model

A contact model is needed as a reference model in the observation process. It connects a state value $\boldsymbol{x}_k$ and the joint measurement $\boldsymbol{q}_k$ to a hypothetical contact situation, which provides information about the expected measured torques. The model is based on our improved implementation [15] of VPS [14]. The basics of VPS are visualized in Fig. 3 for a simplified contact situation. A cylindrical object is pressed on a flat surface, which induces a wrench $\boldsymbol{w}_k$ in the contact. The virtual model represents the wrench in form of the force $\tilde{\boldsymbol{w}}_k$, which acts on the intersecting volume of the virtual representations of the objects, and is in its physical meaning comparable to the buoyant force [18]. While this is a simplification of the possible effects in a real contact, the directions of the virtual wrenches provide reasonable information for the comparison of various contact hypotheses. The VPS implementation approximates the force by the help of so-called pointshells and voxmaps, which are, respectively, discretizations of the geometry in surface points including surface normals and cubic volume elements which conform signed distance fields. These data structures are generated from CAD for arbitrary complex parts.

Dependent on the relative pose $\boldsymbol{H}_k$ of the objects, the virtual contact model provides the contact forces and torques $\tilde{\boldsymbol{w}}_k(\boldsymbol{H}_k) = (\tilde{\boldsymbol{F}}_k^T, \tilde{\boldsymbol{M}}_k^T)^T \in \mathbb{R}^6$, and additionally the contact distance between the virtual objects $\tilde{d}_k = \tilde{d}(\boldsymbol{H}_k) \in \mathbb{R}$. The contact distance defines implicitly the relative configuration space $\tilde{\mathcal{C}}$ between the virtual representations of the MO and EO:

$$\begin{cases} \textit{no contact } (\boldsymbol{H}_k \in \tilde{\mathcal{C}}): & \tilde{d}_k < 0 \\ \textit{contact } (\boldsymbol{H}_k \in \partial\tilde{\mathcal{C}}): & 0 \le \tilde{d}_k < d_t \\ \textit{invalid } (\boldsymbol{H}_k \notin \tilde{\mathcal{C}}): & d_t < \tilde{d}_k, \end{cases} \tag{3}$$

where $d_t > 0$ is a threshold on the maximal feasible virtual penetration. As no additional force/torque-measurement device will be used, $\tilde{\boldsymbol{w}}_k$ is transformed to a virtual contact torque $\tilde{\boldsymbol{\tau}}_k$ according to Eq. (2).

C. Framework for Contact Task Observation

At each time step k the robot provides the measurements $\boldsymbol{y}_k = (\boldsymbol{q}_k, \boldsymbol{\tau}_k)$. The observation model uses this sensory information together with the contact model in order to estimate the current state value $\boldsymbol{x}_k$. Formulated in terms of Bayesian estimation, the objective is to infer the current state distribution density $p(\boldsymbol{x}_k|\boldsymbol{y}_{0:k})$ given the set of past measurements $\boldsymbol{y}_{0:k} = \{\boldsymbol{y}_0, \ldots, \boldsymbol{y}_k\}$. Changes in the contact state are in general nonlinear and the distributions of the uncertain state are not completely describable by methods based solely on Gaussian distributions. Therefore, the observation is carried out with a SMC approach, which can deal with nonlinear and non-Gaussian systems, compare [1] and [2] for a general introduction. A main idea of SMC is that probability densities, like the posterior density $p(\boldsymbol{x}_k|\boldsymbol{y}_{0:k})$, are approximated by a set of samples or so-called particles instead of using continuous model functions. The general procedure of the applied SMC algorithm for assembly observation is visualized in Fig. 4.

The relevant uncertainty space is initially approximated by a set of N samples $\{\boldsymbol{x}_0{}^{(i)}\}$, followed by sequential processing of the set. The basic SMC algorithm for filtering, as it is described by [2], consists of a sampling or propagation step, a weighting and a resampling step. In the first step, samples are drawn from an importance distribution $q(\boldsymbol{x}_k|\boldsymbol{y}_k, \boldsymbol{x}_{k-1}{}^{(i)})$. A commonly used importance model for the estimation of geometric uncertainties assumes a normal distributed random diffusion of the samples, e.g. [3] and [8],

$$q(\boldsymbol{x}_k|\boldsymbol{x}_{k-1}) = \mathcal{N}(\boldsymbol{x}_k|\boldsymbol{x}_{k-1}, \Sigma_{\boldsymbol{x}_k}), \tag{4}$$

with the covariance matrix $\Sigma_{\boldsymbol{x}_k}$. In stiff and accurate kinematic systems, the geometric uncertainties are often rather constant parameter values and the sampling step produces mainly artificial noise in order to avoid particle impoverishment [8]. This random diffusion model will be compared to two further propagation models, which will be presented in the next section in more detail.

The second step is the weighting step, in which the samples obtain weights $W_k{}^{(i)}$ according to their consistency

with the observation

$$W_k^{(i)} \propto \frac{g(\boldsymbol{y}_k|\boldsymbol{x}_k^{(i)}) f(\boldsymbol{x}_k^{(i)}|\boldsymbol{x}_{k-1}^{(i)})}{q(\boldsymbol{x}_k^{(i)}|y_k, \boldsymbol{x}_{k-1}^{(i)})}. \tag{5}$$

Here, $g(\boldsymbol{y}_k|\boldsymbol{x}_k)$ is the observation density and $f(\boldsymbol{x}_k|\boldsymbol{x}_{k-1})$ the transition density of the (hidden) system dynamics. Choosing $q(\boldsymbol{x}_k|\boldsymbol{y}_k, \boldsymbol{x}_{k-1}) = f(\boldsymbol{x}_k|\boldsymbol{x}_{k-1})$ leads to the classic weight computation proposed in the bootstrap filter, compare [1]:

$$W_k^{(i)} \propto g(\boldsymbol{y}_k|\boldsymbol{x}_k^{(i)}). \tag{6}$$

In the presented approach, the observation density distribution consists of two factors. First, the measured torques $\boldsymbol{\tau}_k$ are compared to the virtual contact torques provided by the VPS algorithm assuming normal distributed errors in the measurements:

$$p_{\boldsymbol{\tau}}(\boldsymbol{\tau}_k|\boldsymbol{x}_k^{(i)}) = \mathcal{N}(\boldsymbol{\tau}_k|\tilde{\boldsymbol{\tau}}_k^{(i)}, \Sigma_{\boldsymbol{\tau}}). \tag{7}$$

Compared to other approaches, where the residuum is calculated in the wrench space, cf. [4] and [6], a formulation in joint space is chosen in order to directly refer to the errors in the joint torque measurements and in order to avoid the nonuniform metrics of the wrench space. Second, the contact distance is used to filter out the impossible configurations that violate the relative configuration space between the objects:

$$p_{\boldsymbol{q}}(\boldsymbol{q}_k|\boldsymbol{x}_k^{(i)}) = (\sigma_d\sqrt{2\pi})^{-1} \cdot \begin{cases} 1, & \boldsymbol{H}_k^{(i)} \in \tilde{\mathcal{C}} \\ \exp(-\frac{(\tilde{d}_k - d_t)^2}{(2\sigma_d^2)}), & \boldsymbol{H}_k^{(i)} \notin \tilde{\mathcal{C}}. \end{cases} \tag{8}$$

This density ensures that the virtual objects stay in the valid configuration space given by the threshold d_t on the virtual contact distance $\tilde{d}_k$. The usage of a contact distance in the update step is also described by [6], where combinations of relevant elemental contacts for a given discrete contact state are evaluated. [9] proposes a combination of distance measures in the inhand-localization of objects with robotic hands, which incorporates the information from tactile sensing in a further zero-mean Gaussian distance density. In contrast, the tactile information is explicitly considered in the torque residuum Eq. (7) above. Thus, also the direction of the contact forces are evaluated and certain contact states can be distinguished, which is important for the convergence of the filter in the peg-in-hole task. Under the assumption of independence, the total observation density is then given by the product:

$$g(\boldsymbol{y}_k|\boldsymbol{x}_k^{(i)}) = p_{\boldsymbol{q}}(\boldsymbol{q}_k|\boldsymbol{x}_k^{(i)}) \ \cdot \ p_{\boldsymbol{\tau}}(\boldsymbol{\tau}_k|\boldsymbol{x}_k^{(i)}). \tag{9}$$

Finally, the weights are used in the resampling step in order to select best fitting hypotheses with a higher probability. Expected values of a function $V(\boldsymbol{x}_k)$ can be approximated by the evaluation of the particle distribution:

$$\langle V_k \rangle \approx \sum_{i=1}^{N} W_k^{(i)} V(\boldsymbol{x}_k^{(i)}), \tag{10}$$

which can be used to indicate the current progress of the assembly process and to infer further information from the current state. Note that after resampling, the weights are set to $W_k{}^{(\mathrm{i})} = 1/N$.

III. Sampling Policies

In this section alternative sampling policies for the propagation step of the observer are introduced. They are known from PRM and increase the sample density at the border and in narrow passages of the configuration space $\mathcal{C}$. In the context of contact task observation, it is expected that they decrease the number of required samples for convergence of the estimates and reduce the effects of sample impoverishment.

A. Pure Diffusion Sampling

The first policy is based on the random diffusion model, which was already presented shortly in the previous section, see Eq. (4). It is a default model for unknown or uncertain state dynamics. The samples are propagated according to a given covariance matrix $\Sigma_{\boldsymbol{x},p}$:

function PureDiffusion($\boldsymbol{x}_{k-1}{}^{(\mathrm{i})}$)
  $\boldsymbol{x} \leftarrow \mathcal{N}(\boldsymbol{x}_k|\boldsymbol{x}_{k-1}{}^{(\mathrm{i})}, \Sigma_{\boldsymbol{x},p})$.
  return $\boldsymbol{x}$

If no joint torque is measurable, then the samples will evolve in a diffusion process governed by $\Sigma_{\boldsymbol{x},p}$. In this sampling model, no contact information is evaluated with the advantage of a fast implementation. The diffusion is limited in the constrained regions through the observation density given by Eq. (8) in the update step of the observer.

B. Gaussian Sampler

The Gaussian sampler is known from robot motion planning with PRM [12]. It concentrates samples close to $\partial\mathcal{C}$ by selecting only samples for which a second sample outside of $\mathcal{C}$ can be found within a certain distance. In the here presented work, the method is adapted to concentrate the samples in $\partial\tilde{\mathcal{C}}$ as defined in (3). Therefore, the function EvaluateContact tests whether a sample with state $\boldsymbol{x}$ is within the configuration space of the virtual contact model:

function EvaluateContact($\boldsymbol{x}$, $\boldsymbol{q}_k$)
  if $d_t < \tilde{d}(\boldsymbol{x}, \boldsymbol{q}_k)$ **then**
    return *invalid*
  else if $0 \leq \tilde{d}(\boldsymbol{x}, \boldsymbol{q}_k) < d_t$ **then**
    return *contact*
  else if $\tilde{d}(\boldsymbol{x}, \boldsymbol{q}_k) < 0$ **then**
    return *no contact*

The return value is used to decide on the propagation strategy. If a sample A is already in *contact* it will be propagated according to the PureDiffusion-function above. If the sample A is not in *contact*, a second sample B is drawn according to a distance measure. This is repeated until the locally sampled B is in *contact* or a maximal number of trials L_{max} is reached. This sampling policy is applied for every hypothesis $\boldsymbol{x}_{k-1}{}^{(\mathrm{i})}$ and is summarized as:

function GaussianSampler($\boldsymbol{x}_{k-1}{}^{(\mathrm{i})}$, $\boldsymbol{q}_k$)
  $\boldsymbol{x}_A := \boldsymbol{x}_{k-1}{}^{(\mathrm{i})}$
  $A \leftarrow$ EvaluateContact($\boldsymbol{x}_A, \boldsymbol{q}_k$)
  if $A \neq$ *contact* **then**
    for j := 1 to L_{max} **do**
      $\boldsymbol{x}_B \leftarrow \mathcal{N}(\boldsymbol{x}_B|\boldsymbol{x}_{k-1}{}^{(\mathrm{i})}, \Sigma_{\boldsymbol{x},g})$.

```
        B ← EVALUATECONTACT(x_B, q_k)
        if B = contact then
            return x_B
    return PUREDIFFUSION(x_A)
```

In contrast to the classical policy of [12], the samples A are not discarded completely in the case that the collision conditions are not satisfied, but rather resampled locally. L_{max} controls the effort in order to find a solution and finally how dense the border will be filled with samples. For $L_{max} \rightarrow \infty$ all samples will be concentrated in $\partial\tilde{\mathcal{C}}$; for small values of L_{max} the pure diffusion dominates the sample propagation. The parameter $\Sigma_{\boldsymbol{x},g}$ controls the search distance in the local resampling loop.

C. Bridge Test Sampling

The following policy is also motivated by PRM. The RBB [13] favors samples in narrow passages of the configuration space. The method is also adopted for the propagation context. Here again, a second sample B is created for a initial hypothesis A:

```
function BRIDGETEST(x_{k-1}^(i), q_k)
    x_A := x_{k-1}^(i)
    for j := 1 to L_max do
        x_B ← N(x_B | x_A, Σ_{x,b}).
        B ← EVALUATECONTACT(x_B, q_k)
        if B = invalid then
            x_C ← (x_A + x_B)/2
            C ← EVALUATECONTACT(x_C, q_k)
            if C ≠ invalid then
                return x_C
    return PUREDIFFUSION(x_A)
```

In the case B is $invalid$, a bridge point C will be created which is located at the half distance between A and B. If this bridge point is valid, i.e. $contact$ or $no\ contact$, it will be propagated as the new hypothesis. This pulls samples into the narrow passages of the local configuration space. The covariance matrix $\Sigma_{\boldsymbol{x},b}$ is related to the gap size of the expected narrow passages. Here, a Gaussian density is chosen. As the authors of [13] note, if prior knowledge about the narrow passage is available, a more suitable function could be used. Similarly to the GAUSSIANSAMPLER-function a higher number of maximal iterations L_{max} increases the admissible effort, but also the density in the narrow passage.

IV. EXPERIMENTS AND RESULTS

The three sampling policies are validated based on measurements obtained from the KUKA LBR iiwa robot, which is the new industrial version of the LWR developed by [19]. The observation is carried out for a peg-in-hole task, where an aluminum profile is inserted in an assembly fixture (Fig. 1). The profile is tilted, aligned and inserted with enabled impedance control mode, which allows implementing a robust assembly strategy. Nevertheless, an observation of the process is requested in flexible production facilities, as the workcell setup is not guaranteed to be fixed and high-level monitoring and decisions are desired.

A. Experimental Setup

The peg-in-hole task is part of a larger assembly testbed previously shown at AUTOMATICA 2014[1]. The MO is a 200 mm long 40 mm × 40 mm aluminum profile of the *item MB Building Kit System*[2] and the EO is the assembly fixture, which provides form-closure with the longitudinal slots of the profile at two sides. The depth of the fixture is 100 mm, the clearance is below 1 mm. The voxmap of the EO in the VPS has a resolution of 1 mm, and the pointshell of the MO contains in total 5666 points. A world model [20] provides the assumed pose of the fixture relative to the robot base $\boldsymbol{H}_{B\bar{C}}$ and the grasp transformation $\boldsymbol{H}_{AD}$. The desired goal pose at the bottom of the fixture is given by the nominal transformation $\boldsymbol{H}_{CD,goal}$. Measurements of the current joint pose $\boldsymbol{q}_k$ and the torque $\boldsymbol{\tau}_k$ are taken at a rate of 33 Hz and evaluated offline in order to compare the effects of the sampling policies.

B. Simulated Sample Evolution at Narrow Passage

Simulations are carried out in order to validate the spread of the samples. Therefore, the relative transformation $\boldsymbol{H}_{CD}$ is kept constant at the entrance of the narrow passage at ${}_{C}x_{CD} = 95$ mm (Fig. 5). In this configuration, no torque is measured and the samples mainly evolve according to the propagation model and the boundaries of the configuration space. In the given example, the threshold on the maximal penetration is set to $d_t = 2$ mm and the number of allowed iterations is $L_{max} = 5$. Position uncertainties $\boldsymbol{x} = {}_{C}(x, y, z)_{\bar{C}C}$ of the fixture relative to its assumed pose are considered here to show the basic results. The initial samples are uniformly drawn from a cubic uncertain volume around $\bar{C}$ with a side length of 20 mm and a shifted mean of one third of the dimensions. The covariance matrices are assumed to be diagonal $\Sigma_{\boldsymbol{x}} = \mathrm{diag}(\sigma_x^2, \sigma_y^2, \sigma_z^2)$ with $\sigma_x = \sigma_y = \sigma_z = \sigma$. For the pure diffusion sampling is chosen $\sigma = \sigma_p = 0.1$ mm, for the Gaussian sampler $\sigma = \sigma_g = 2$ mm, and for the bridge test $\sigma = \sigma_b = 6$ mm. The Gaussian sampler should place the samples close to the border, therefore, we set $\sigma_g \leq d_t$. The bridge test apparently requires a high mobility of the samples in order to build a bridge in the narrow passage, thus $\sigma_b \geq 2d_t$ provides reasonable results.

On the right side of Fig. 5, the evolution is displayed as the history of $N = 1000$ samples within 10 repetitions of the observer cycle. The pure diffusion case shows an almost uniform distribution in the free space The Gaussian sampler captures samples near $\partial\tilde{\mathcal{C}}$, whereas the bridge test policy increases significantly the density at the entrance of the narrow passage and also near the border of the configuration space. Although obtained in simulation and with local resampling, these results show clearly the increased sample density in the critical regions as expected from the known analysis of [12] and [13].

[1] Video: http://youtu.be/2jYhdmk-pMg

[2] item Industrietechnik GmbH, http://www.item24.de

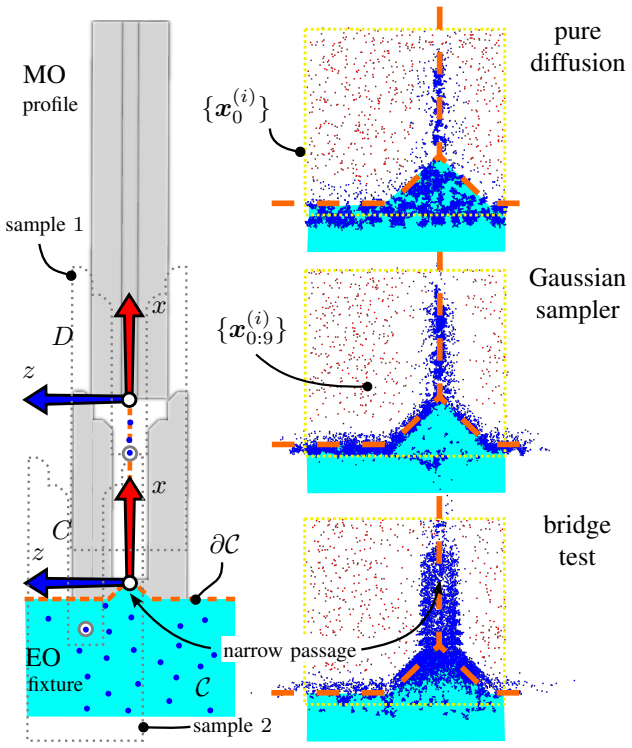

Fig. 5. The sampling policies at the entrance of the narrow passage. Here in simulation, the pose of the profile is kept constant, while the samples evolve. Note that each drawn dot represents a sample of the relative configuration space $\tilde{\mathcal{C}}$ at time k, i.e. a hypothetical pose of the fixture. Blue dots denote samples in $\tilde{\mathcal{C}}$, red marked samples violate $\tilde{\mathcal{C}}$. The yellow dotted line encloses the initial sample set $\{\boldsymbol{x}_0{}^{(i)}\}$. The orange dashed line visualizes the ideal border $\partial\mathcal{C}$, which is approximated by the sample distribution. Sample 1 is in the narrow passage, sample 2 in free space.

C. Peg-in-Hole Experiment

In the observation of the real assembly process, the sample evolution is additional affected by the measured joint torques dependent on the phase of the assembly process. The process is visualized in Fig. 6 together with the distribution of the state samples with the bridge test as propagation function. The task execution and exemplary results are also presented in the video attachment. Like above, the samples condense at the entrance of the narrow passage in the configuration space. An exemplary evolution of all state variables is plotted in Fig. 7 for the three policies, with $N = 1000$. All distributions shrink when the profile is close to the narrow passage of the fixture at $k \approx 25$. At $k \approx 60$ the profile enters the more constrained region, where the slots at the sides are aligned inside with the fixture; at $k \approx 170$ the peg reaches the bottom. The sample populations of the Gaussian sampler and the bridge test show a faster filling of the narrow passage after an intermediate contraction during the alignment. Whereas the sample population for the pure diffusion is spreading only slowly and concentrated in clusters, thus indicating a stronger influence of sample impoverishment and a worse coverage of the relevant configuration space.

For the further evaluation of convergence and robustness,

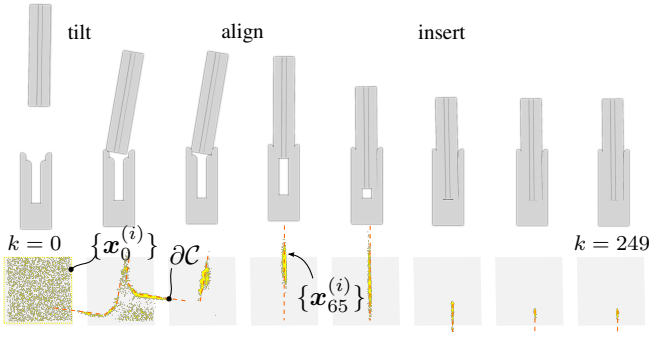

Fig. 6. The evolution of the samples based on measurements from the real assembly process for the bridge test propagation ($N = 1000$, front-view), as also presented in the video attachment. The dotted line encloses the initial sample set $\{\boldsymbol{x}_0{}^{(i)}\}$, whereas the single yellow dots represent the sample set $\{\boldsymbol{x}_k{}^{(i)}\}$ at time k. The samples condense at $\partial\tilde{\mathcal{C}}$, the border region of the local configuration space (orange dashed line).

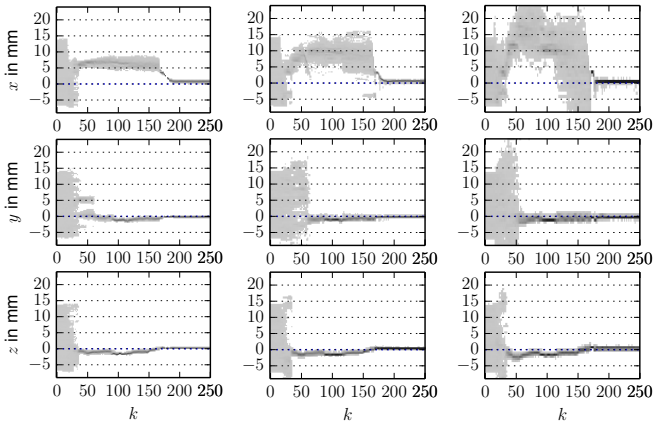

(a) pure diffusion (b) Gaussian sampler (c) bridge test

Fig. 7. Exemplary sample evolution for the three propagation sampling policies ($N = 1000$). The sampled distribution of the state $\boldsymbol{x} = {}_{\bar{C}}(x, y, z)_{\bar{C}C}$ over the time step k is shown. All distributions condense when the profile is close to the narrow passage of the fixture at $k \approx 25$. Dark gray values indicate a high sample density. The x-values of the samples are distributed wider for the bridge test policy after $k \approx 100$, which features an improved filling of the narrow passage during the insertion of the profile.

the insertion is recorded 5 times and evaluated multiple-times for each policy and each number of samples on a logarithmic scale $N \in \{10, 32, 100, 316, 1000, 3162\}$. The propagation models are equally parametrized like in Section IV-B. In the observation model, it is assumed that the measurement errors of the torques are independent for each joint. Therefore, a diagonal covariance matrix $\Sigma_{\boldsymbol{\tau}} = \mathrm{diag}(\sigma_\tau^2, \ldots, \sigma_\tau^2)$ is chosen in the observation density of the joint torques. With $\sigma_\tau = 5\,\mathrm{Nm}$, a large tolerance with respect to unmodeled effects and errors in the torque measurements is given. The residuum of the contact distance is $\sigma_d = 0.1\,\mathrm{mm}$.

For the analysis of the error in the observation, a goal pose $\boldsymbol{H}_{DC,goal}$ without clearance is assumed and therefore a uni-modal target distribution of the samples is present. The ground truth of the transformation at the end of the assembly process is given with

$$\boldsymbol{H}_{\bar{C}C,ground} := \boldsymbol{H}_{\bar{C}B}\boldsymbol{H}_{BA}(\boldsymbol{q}_{end})\boldsymbol{H}_{AD}\boldsymbol{H}_{DC,goal}, \quad (11)$$

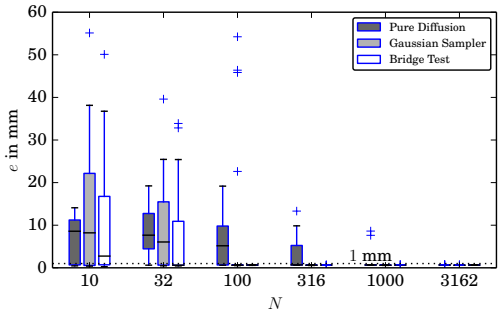

Fig. 8. Boxplot of errors with respect to the ground truth at the final observation step. A set of 5 records is evaluated 5 times for each policy and each value of sample number N. The error decrease with increased N. The bridge test shows consistent valid results with $e < 1\,\text{mm}$ for $N \geq 100$, the Gaussian sampler for $N \geq 316$, the pure diffusion sampler for $N \geq 3162$,

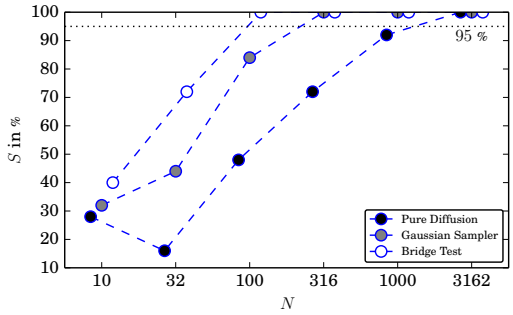

Fig. 9. Reliability S measured by the percentage of observations with $e < e_t = 1\,\text{mm}$ over N. For each sample number N and each policy, a set of 5 records is evaluated 5 times; the reliability is calculated with respect to the total number of evaluations, e.g. the bridge test shows reliable results with $S > 95\,\%$ for $N \geq 100$.

where the peg has successfully reached the goal pose and the robot configuration is $\boldsymbol{q}_{end}$, obtained from the joint measurements. With the help of Eq. (10), the expected value of the transformation from the assumed pose of the fixture to the observed value $\langle \boldsymbol{H}_{\bar{C}C}(\boldsymbol{x}_k) \rangle$ can be obtained. The error at the final observation step is then calculated by

$$e = ||\langle \boldsymbol{r}_{\bar{C}C}(\boldsymbol{x}_k) \rangle - \boldsymbol{r}_{\bar{C}C,ground}||_2, \tag{12}$$

with $\boldsymbol{r}_{\bar{C}C} \in \mathbb{R}^3$, the position component of $\boldsymbol{H}_{\bar{C}C}$. Fig. 8 shows the error for the policies for the repeated evaluations over the same sample number N and Fig. 9 the reliability measured by the percentage S of observations with $e < e_t = 1\,\text{mm}$. None of the policies show a reliable convergence for low numbers of particles $N < 100$ as $S < 95\,\%$. For $N \leq 100$, the Gaussian sampler and the bridge test appear to have the highest spread in the error distribution, which is due to the higher mobility of the samples ($\sigma_g, \sigma_b > \sigma_p$) and the potential to favor alternative narrow passages if the initial density is not sufficient. The error converges finally at $e \approx 0.5\,\text{mm}$ for all policies and $N > 1000$. The minimal required number of samples for a significant reliability of the convergence is different. The observations made with the pure diffusion model requires high sample numbers above $N > 1000$ for $S > 95\,\%$. A considerably lower number is achieved with the bridge test policy, where the expected value of the error is already close to the achievable accuracy at $N = 100$ and $S > 95\,\%$. The results of the Gaussian sampler lie in between.

V. Discussion

In the previous section, it was shown that the number of required samples needed for convergence can be reduced significantly by the application of more advanced sampling strategies in the propagation step of the SMC filter. The number of required samples could be reduced by a factor of $f \approx 1/10$ if the bridge test is applied instead of the pure diffusion model. The benefit of using the Gaussian sampler is comparable, but slightly smaller. The question is whether the computational effort introduced by the additional collision checks in the propagation model is feasible. In an optimal implementation of the observation algorithm, most time is spent in the collision checks. The update model needs a single call of VPS in the weighting of a sample according to the distance and torque consistency; in the worst case, further $L_{max} + 1$ calls are required in the propagation step of the Gaussian sampler and $2 \cdot L_{max}$ calls in the bridge test. Under these assumptions and given a sequential processing of the samples, the total time of a single observation step with N samples is:

$$T_{p,max} \approx N \cdot T_{vps}, \tag{13}$$
$$T_{g,max} \approx (L_{max} + 2) \cdot f \cdot N \cdot T_{vps}, \tag{14}$$
$$T_{b,max} \approx (2 \cdot L_{max} + 1) \cdot f \cdot N \cdot T_{vps}, \tag{15}$$

for the pure diffusion model, the Gaussian sampler, and the bridge test. The average time needed for a single contact computation is denoted as T_{vps}. In the given example with $N = 1000$ samples and $L_{max} = 5$ and $T_{vps} \approx 1\,\text{ms}$, we obtain $T_{p,max} = 1\,\text{s}$, $T_{g,max} = 0.7\,\text{s}$ and $T_{b,max} = 1.1\,\text{s}$. In the worst case, the advantages of the alternative policies in the needed computational time are not directly visible, but assuming that in average less than L_{max} iterations are required, an improvement can be achieved. Table I shows the actual rate of processed particles per second (pps) and the effective rate which incorporates the reduction of required particles averaged over all exemplary evaluations. An effective speedup of ≈ 2.5 is achieved by the bridge test, and ≈ 6 by the Gaussian sampler, when the reduced number of required samples is incorporated. A comparison to the performance of [8] is not directly possible as they use simpler geometries for probing, and the application for a peg-in-hole with more complex geometries is only given as an outlook. Nevertheless, the combination of the approach with a RBPF is reasonable when also orientation uncertainties are incorporated.

TABLE I

Rate of processed particles per second.

propagation model	actual rate	reduction factor f	effective rate
pure diffusion	180 pps	1.0	180 pps
Gaussian sampler	110 pps	0.1	1100 pps
bridge test	45 pps	0.1	450 pps

In any case, a general speedup of the computation is necessary in order to accomplish an online observation of the assembly process. The current implementation does not run in real-time, but also does not yet use the potential of an optimized implementation and a parallelized architecture for which a speedup greater than 10 is technically feasible; compare [21] for an analysis of the theoretical speedup in the distributed implementation of SMC algorithms. Therefore, a minimal observation rate of 10 Hz seems likely in the current scenario. This rate might be too low for the direct usage as input in the lower torque level controllers of the robot, but is sufficient for high level task control and reasoning in future applications. Especially the larger volume of samples within the narrow passage increases the knowledge about the local configuration space which might be exploited for parametrization of low level controllers, e.g. the stiffness of the impedance controller could be adapted according to the current phase of the insertion of the peg and the shape of the local configuration space. And of course, also the quality of repetitive tasks can be improved when initially uncertain goal frames are updated by the assembly observation system.

VI. Conclusions

An observation method based on SMC was presented, which improves the capability of a robot system to use joint torque sensing as an input for the observation of robotic assembly tasks. It makes use of the fast haptic rendering algorithm VPS for complex geometrical objects and therefore is suitable for a large variety of assembly parts. The observation method was evaluated with joint torque measurements obtained from a peg-in-hole assembly with a LWR robot arm. Especially it was shown how samples of the uncertain space can be dragged into narrow passages of the configuration space in order to increase the sample density in these critical areas. Thus, the number of total samples needed for convergence can be reduced significantly and a local sampled map of the configuration space can be obtained. This information can be used in future high-level controllers in order to adapt strategies to the current execution. The potential of using these sampling methods in the propagation step of the observation was demonstrated, but further investigations have to be carried out in order to weight the benefits against the time constraints that are given in the real process. Further analysis is required in the presence of large relative orientational errors, as only results on position uncertainties were presented here. In addition, alternative adaptive methods should be investigated, which could improve the performance of the observation more efficiently.

Acknowledgment

The research leading to these results has received funding from the European Union Seventh Framework Programme (FP7/2007-2013) under grant agreement no. 287787, project SMErobotics.

References

[1] O. Cappé, S. J. Godsill, and E. Moulines, "An overview of existing methods and recent advances in sequential monte carlo," *Proc. of the IEEE*, vol. 95, no. 5, pp. 899 – 924, 2007.

[2] A. Doucet and A. M. Johansen, "A tutorial on particle filtering and smoothing: fifteen years later," *Handbook of Nonlinear Filtering*, vol. 12, pp. 656–704, 2009.

[3] S. Chhatpar and M. Branicky, "Localization for robotic assemblies using probing and particle filtering," in *Adv. Intelligent Mechatronics. Proc., 2005 IEEE/ASME Int. Conf. on*, July 2005, pp. 1379–1384.

[4] U. Thomas, S. Molkenstruck, R. Iser, and F. Wahl, "Multi sensor fusion in robot assembly using particle filters," in *Robotics and Automation, 2007 IEEE Int. Conf. on*, April 2007, pp. 3837–3843.

[5] P. Tang and J. Xiao, "Automatic generation of high-level contact state space between 3d curved objects," *The Int. Journal of Robotics Research*, vol. 27, no. 7, 2008.

[6] W. Meeussen, J. Rutgeerts, K. Gadeyne, H. Bruyninckx, and J. De Schutter, "Contact-state segmentation using particle filters for programming by human demonstration in compliant-motion tasks," *IEEE Transactions on Robotics*, vol. 23, no. 2, pp. 218–231, 2007.

[7] K. Hertkorn, M. Roa, C. Preusche, C. Borst, and G. Hirzinger, "Identification of contact formations: Resolving ambiguous force torque information," in *Robotics and Automation (ICRA), 2012 IEEE Int. Conf. on*, May 2012, pp. 3278–3284.

[8] Y. Taguchi, T. Marks, and H. Okuda, "Rao-blackwellized particle filtering for probing-based 6-dof localization in robotic assembly," in *Robotics and Automation (ICRA), 2010 IEEE Int. Conf. on*, May 2010, pp. 2610–2617.

[9] M. Chalon, J. Reinecke, and M. Pfanne, "Online in-hand object localization," in *Intelligent Robots and Systems (IROS), 2013 IEEE/RSJ Int. Conf. on*, Nov 2013, pp. 2977–2984.

[10] L. E. Zhang and J. C. Trinkle, "The application of particle filtering to grasping acquisition with visual occlusion and tactile sensing," in *Proc. of the 2012 IEEE Int. Conf. on Robotics and Automation*. IEEE, 2012, pp. 3805–3812.

[11] L. E. Kavraki, P. Svestka, J.-C. Latombe, and M. Overmars, "Probabilistic roadmaps for path planning in high dimensional configuration spaces," *IEEE Transactions on Robotics and Automation*, vol. 12, no. 4, pp. 566–580, 1996.

[12] V. Boor, M. Overmars, and A. van der Stappen, "The gaussian sampling strategy for probabilistic roadmap planners," in *Robotics and Automation, 1999. Proc.. 1999 IEEE Int. Conf. on*, vol. 2, 1999, pp. 1018–1023 vol.2.

[13] Z. Sun, D. Hsu, T. Jiang, H. Kurniawati, and J. Reif, "Narrow passage sampling for probabilistic roadmap planning," *IEEE Trans. on Robotics*, vol. 21, no. 6, pp. 1105–1115, Dec 2005.

[14] W. A. McNeely, K. D. Puterbaugh, and J. J. Troy, "Six degree-of-freedom haptic rendering using voxel sampling," in *ACM SIGGRAPH 2005 Courses*, ser. SIGGRAPH '05. New York, USA: ACM, 2005.

[15] M. Sagardia, T. Stouraitis, and J. a. Lopes e Silva, "A new fast and robust collision detection and force computation algorithm applied to the physics engine bullet," in *Conf. and Exhibition of the European Association of Virtual and Augmented Reality (EuroVR)*, 2014.

[16] A. Stemmer, A. Albu-Schäffer, and G. Hirzinger, "An analytical method for the planning of robust assembly tasks of complex shaped planar parts," in *Proc. of the 2007 IEEE Int. Conf. on Robotics and Automation*. IEEE, 2007, pp. 317 – 323.

[17] J. De Schutter, T. De Laet, J. Rutgeerts, W. Decr, R. Smits, Aertbelin, K. Claes, and H. Bruyninckx, "Constrained-based task specification and estimation for sensor-based robot systems in the presence of geometric uncertainty," *The Int. Journal of Robotics Research*, vol. 26, no. 5, pp. 433–455, 2007.

[18] J. Barbič, "Real-time reduced large-deformation models and distributed contact for computer graphics and haptics," Ph.D. dissertation, Carnegie Mellon University, 2007.

[19] A. Albu-Schäffer, S. Haddadin, C. Ott, A. Stemmer, T. Wimböck, and G. Hirzinger, "The DLR lightweight robot: design and control concepts for robots in human environments," *Industrial Robot: An Int. Journal*, vol. 34, no. 5, pp. 376–385, 2007.

[20] D. Leidner, C. Borst, and G. Hirzinger, "Things are made for what they are: Solving manipulation tasks by using functional object classes," in *Humanoid Robots,12th IEEE-RAS Int. Conf. on*, 2012, pp. 429–435.

[21] A. Bashi, V. Jilkov, R. Li, and H. Chen, "Distributed implementations of particle filters," in *Proceedings of the 6th International Conference of Information Fusion*, 2003, pp. 1164–1171.